Time-resolved infrared absorption studies of the solvent-dependent vibrational relaxation dynamics of chlorine dioxide

Joshua C. Bolinger, Teresa J. Bixby, and Philip J. Reid[a)]
Box 351700, Department of Chemistry, University of Washington, Seattle, Washington 98195

(Received 12 May 2005; accepted 20 June 2005; published online 29 August 2005)

We report a series of time-resolved infrared absorption studies on chlorine dioxide (OClO) dissolved in H_2O, D_2O, and acetonitrile. Following the photoexcitation at 401 nm, the evolution in optical density for frequencies corresponding to asymmetric stretch of OClO is measured with a time resolution of 120 ± 50 fs. The experimentally determined optical-density evolution is compared with theoretical models of OClO vibrational relaxation derived from collisional models as well as classical molecular-dynamics (MD) studies. The vibrational relaxation rates in D_2O are reduced by a factor of 3 relative to H_2O consistent with the predictions of MD. This difference reflects modification of the frequency-dependent solvent-solute coupling accompanying isotopic substitution of the solvent. Also, the geminate-recombination quantum yield for the primary photofragments resulting in the reformation of ground-state OClO is reduced in D_2O relative to H_2O. It is proposed that this reduction reflects enhancement of the dissociation rate accompanying vibrational excitation along the asymmetric-stretch coordinate. In contrast to H_2O and D_2O, the vibrational-relaxation dynamics in acetonitrile are not well described by the theoretical models. Reproduction of the optical-density evolution in acetonitrile requires significant modification of the frequency-dependent solvent-solute coupling derived from MD. It is proposed that this modification reflects vibrational-energy transfer from the asymmetric stretch of OClO to the methyl rock of acetonitrile. In total, the results presented here provide a detailed description of the solvent-dependent geminate-recombination and vibrational-relaxation dynamics of OClO in solution. © *2005 American Institute of Physics*. [DOI: 10.1063/1.2000234]

I. INTRODUCTION

The photochemistry of chlorine dioxide (OClO) is of interest due to the participation of this species in atmospheric chemistry, and, in particular, as a reservoir species for atomic chlorine.[1–4] The following reaction pathways are available to OClO following photoexcitation resonant with the $^2B_1$-$^2A_2$ electronic transition:

$$\text{(i)} \quad \mathrm{OClO} \xrightarrow{h\nu} \mathrm{ClO}(^2\Pi) + \mathrm{O}(^3P_g),$$

$$\text{(ii)} \quad \mathrm{OClO} \xrightarrow{h\nu} \mathrm{Cl}(^2P_u) + \mathrm{O_2}(^1\Delta_g, {}^3\Sigma_g^-),$$

$$\text{(iii)} \quad \mathrm{OClO} \xrightarrow{h\nu} \mathrm{ClOO} \xrightarrow{\Delta} \mathrm{Cl}(^2P_u) + \mathrm{O_2}(^3\Sigma_g^-, {}^1\Delta_g).$$

For gaseous OClO, the predominant photochemical pathway is the production of ClO and O [pathway (i)], with the quantum yield for atomic chlorine production (Φ_{Cl}) having a maximum value of ~ 0.04.[5–8] In aqueous solution, Φ_{Cl} increases to 0.1[1,9–18] and approaches unity in low-temperature matrices.[15,16,18–20] Understanding the role of the solvent in defining Φ_{Cl} is a central issue in OClO photochemistry in condensed environments.

Since $\Phi_{\mathrm{Cl}} = 0.1$ in aqueous solution, the production of ClO and O remains the dominant photochemical pathway in this phase, but the reaction dynamics along this pathway are modified relative to the gas phase by two phenomena: intermolecular-vibrational relaxation and geminate recombination. Insight into both phenomena has been provided by time-resolved absorption and resonance Raman (TRRR) spectroscopy.[10,12,13,21–24] These studies have established that in aqueous solution the quantum yield for OClO reformation by OCl and O recombination is 0.9, and that this yield is solvent dependent. Recombination of the primary photofragments occurs on the subpicosecond time scale. The TRRR studies have shown that following OClO photoexcitation, the photoinduced depletion in Stokes scattering intensity for transitions involving the OClO symmetric stretch recovers with two-time constants: a subpicosecond component corresponding to recombination and a slower, 9-ps component corresponding to intermolecular vibrational relaxation.[24,25] The appearance of anti-Stokes intensity for transitions involving the symmetric stretch was delayed ~ 5 ps relative to the formation of OClO suggesting that excess vibrational energy is initially deposited along another coordinate, presumably the asymmetric stretch. The 5-ps delay in the appearance of anti-Stokes intensity was taken as evidence that intramolecular-vibrational-energy reorganization occurs on this time scale.[1,24,25] This interpretation of the TRRR results is consistent with transient UV-visible absorption studies of aqueous OClO where the temporal evolution in optical density could be reproduced assuming that the asymmetric-stretch coordinate was primarily responsible for the loss of excess vibrational energy to the solvent.[10,12] Since the asym-

a)Author to whom correspondence should be addressed. Electronic mail: preid@chem.washington.edu

metric stretch is not strongly Franck-Condon coupled to the optical transition of interest, transient absorption experiments provide only limited information regarding vibrational-relaxation dynamics along this coordinate. In addition, this coordinate is silent in the resonance Raman spectra of solution-phase OClO. Therefore, spectroscopic techniques that provide a direct measure of vibrational-energy deposition and relaxation along the asymmetric-stretch coordinate are required to ascertain the role of this coordinate in the geminate-recombination and vibrational-relaxation dynamics of OClO.

Theoretical techniques have also been employed to refine our understanding of OClO vibrational-relaxation dynamics in solution.[26–30] Using classical molecular dynamics (MD), Poulsen *et al.* were able to reproduce the lifetime of the first excited vibrational state of the asymmetric stretch through analysis of the solvent-solute force-force correlation function.[31] Benjamin and co-workers have provided a detailed look into the solvent-dependent OClO vibrational-relaxation dynamics by performing the MD simulations in H_2O, D_2O, acetonitrile, and ethanol.[32,33] In this work, relaxation rates from the first excited state along the asymmetric-stretch coordinate to all other lower-energy vibrational states were determined, and good agreement with experiment was observed. However, detailed information regarding the vibrational-relaxation dynamics along the asymmetric-stretch coordinate required to further test the predictions of Benjamin and co-workers was not available at the time of their study. To address this issue, we performed a time-resolved infrared (TRIR) absorption study of OClO in water.[34] In this study, relaxation rates along the asymmetric-stretch vibrational manifold were measured through the $n=8$ vibrational level. The MD results of Benjamin and co-workers were compared to the experimentally determined vibrational-relaxation rates, and qualitative agreement was observed. However, the absolute rates predicted by MD were five times less than those determined by experiment.[34] This difference raises the following question, does this discrepancy in rates exist only for H_2O, or are similar differences observed in other solvents? In our previous TRIR study, the population of levels above $n=8$ along the asymmetric-stretch coordinate was not observed. However, the $\sim 17\,000$ cm^{-1} of excess energy available to OClO following geminate recombination dictates that levels as high as $n=15$ could be populated if all the excess vibrational energy available to OClO upon recombination is deposited along the asymmetric-stretch coordinate.[25] However, probe frequencies resonant with the upper levels of the asymmetric-stretch vibrational manifold overlap with the librational band of water, making measurements in this frequency region quite difficult. By measuring the relaxation dynamics in more transparent solvents, information regarding the relaxation dynamics of higher-energy vibrational states along the asymmetric-stretch coordinate can be obtained.

We present here a series of TRIR absorption studies in which the geminate-recombination and vibrational-relaxation dynamics of OClO are investigated in three solvents: H_2O, D_2O, and acetonitrile. The central results of this study are as follows. The appearance of vibrational energy along the asymmetric-stretch coordinate of OClO in both H_2O and D_2O occurs on the subpicosecond time scale demonstrating that geminate recombination of the primary photofragments occurs on this time scale. The vibrational relaxation rates in D_2O are approximately three times smaller than those in H_2O, in qualitative agreement with the predictions of MD. In acetonitrile, higher vibrational states are available for study given the increased transparency of this solvent, and population of these higher-energy states following geminate recombination is observed. An $\sim$10-ps delay in optical-density evolution relative to photoexcitation is evident, and is proposed to reflect a longer excited-state lifetime in acetonitrile relative to H_2O and D_2O. In H_2O and D_2O, the vibrational-relaxation dynamics are modeled assuming that the relaxation rates reflect the frequency dependence of solute/solvent force-force correlation function consistent with the earlier MD results. However, the relaxation dynamics in acetonitrile are not well reproduced by this approach, potentially reflecting the complex nature of the coupling between the OClO asymmetric-stretch coordinate and specific modes of the solvent. In total, the studies presented here provide a detailed picture of the role of the asymmetric-stretch coordinate in the condensed-phase reaction dynamics of OClO.

II. EXPERIMENT

The laser system employed in these studies has been discussed in detail elsewhere; therefore, only a brief summary is presented here.[34] A regenerative Ti:sapphire amplifier (Spectra Physics) was seeded with a Ti:sapphire oscillator (KM Labs) pumped by the frequency-doubled output of a $Nd:VO_4$ laser (Coherent). The amplifier output consisted of 60-fs pulses centered at 802 nm with a pulse energy of 960 μJ at a repetition rate of 1 kHz. The amplifier output was split into two beams using a 60/40 beamsplitter. The higher-energy beam was used to pump an optical parametric ampliflier (OPA, Quantronix TOPAS), and the signal and idler beams from the OPA were used for difference frequency generation (DFG) in $AgGaS_2$ (type I), to produce the probe field centered at 9.5 μm. The lower-energy beam derived from the amplifier output was frequency doubled using a 100-μm-thick β-BBO crystal (type I) to provide the 401-nm pump field.

The pump field was delivered to a retroreflector mounted on a motorized delay stage to allow for temporal delay of the pump relative to the probe. To minimize the contribution of rotational dynamics to the measured optical-density evolution, the polarization of the pump was oriented to 54.7° relative to the probe using a zero-order half-wave plate. The 20-μJ pump field was weakly focused to a 1.5-mm spot size in the sample. The change in sample optical density was found to vary linearly with pump power. The 9.5-μm probe field was collimated using two parabolic off-axis reflectors, then passed through a ZnSe 50/50 beamsplitter. The transmitted beam used as a reference while the reflected beam was used as the probe. The probe (0.15-μJ per pulse) was focused on the sample using a parabolic off-axis reflector. The spatial and temporal overlap of the pump and probe fields was measured using the change in optical density in a

Si wafer following a 401-nm photoexcitation. The Si response was used to determine the instrument response (120±50-fs full width half maximum).

After passing through the sample, the probe field was recollimated and delivered to a 0.25-m monochromator (Jarrell Ash) equipped with a 100-groove/mm grating blazed at 5.6 μm to isolate individual probe frequency components with a resolution of 30 cm^{-1}. The reference field also passed through the monochromator to ensure that identical spectrum components of the probe and reference were measured. Detection of the probe and reference intensities was accomplished using two LN_2-cooled MCT detectors (Infrared Products). The detector outputs were delivered to separate gated integrators, and the integrator outputs were subtracted on a shot-to-shot basis. A mechanical chopper operating at half the frequency of the amplifier was used to block every other pump pulse, and successive probe signals were subtracted to determine the pump-induced change in the sample optical density. The CaF_2 cell windows demonstrated a nonlinear response to the 400-nm actinic field employed. To remove the contribution of the CaF_2 response from the optical-density evolution assignable to OClO, a biphasic exponential decay with time constants of 0.61 and 2.34 ps was constructed and subtracted from the data. The robustness of this approach was established by performing this procedure for a variety of pump powers, and the resulting evolution in optical density assignable to OClO was not affected. In addition, this process was compared to removal of the CaF_2 response by direct subtraction of the response measured in the absence of OClO, and the resulting evolution in optical density assignable to OClO was in agreement with that obtained using the exponential-decay subtraction procedure.

Samples were prepared by heating potassium chlorate and oxalic acid dihydrate in a 2.4*M* H_2SO_4 (aq) at 60 °C to produce gaseous OClO. The resulting yellow gas passed through a drying tube filled with P_2O_5, and was then bubbled through the solvent of interest. This stock solution was diluted until a concentration of 50 mM was obtained, with the diluted solution used for the experiments reported here. The kinetics reported here was invariant with a twofold reduction in concentration. All reagents and solvents (Fisher Scientific) were of the highest purity available except for D_2O (99%, Cambridge Isotopes). The sample was delivered to a Teflon flow cell (Harrick Scientific) equipped with CaF_2 windows. A 56-μm cell path length was used for H_2O and D_2O, and a 150-μm pathlength was employed in acetonitrile. The time-dependent optical-density evolution was analyzed by fitting the data to a sum of exponentials using the Levenberg-Marquardt algorithm. Goodness of fit was judged using the reduced χ^2 values and by visual inspection of the residuals. Errors reported here represent one standard deviation from the mean as determined from at least four measurements.

III. RESULTS

A. Experimental results and kinetic analysis

Figures 1–3 present the measured evolution in optical density following the photoexcitation of OClO dissolved in H_2O, D_2O, and acetonitrile, respectively. The asymmetric-stretch coordinate of aqueous OClO in the ground $^2B_1$ state has a harmonic frequency of 1105 cm^{-1} and anharmonicity of 11 cm^{-1} such that fundamental transition for this coordinate is at 1094 cm^{-1}. Fourier transform infrared (FTIR) measurements demonstrated that frequency of this transition did not change within experimental error (±2 cm^{-1}) for the solvents studied here (data not shown). The evolution in optical density following OClO photoexcitation was measured at 14-cm^{-1} intervals starting from 1094 cm^{-1} and ending at 1014 cm^{-1} in H_2O and D_2O, or ending at 958 cm^{-1} in acetonitrile. As the probe frequency is reduced, the evolution in optical density provides a measure of the vibrational-relaxation dynamics involving higher-energy states along the asymmetric-stretch vibrational manifold. Probe frequencies at 1094 cm^{-1} through 1080 cm^{-1} demonstrate reductions in optical density consistent with pump-induced depletion of the ground state; therefore, the optical-density evolution at these frequencies provides information involving the lowest-energy levels of the asymmetric-stretch vibrational manifold. Intermediate probe frequencies (1066 and 1053 cm^{-1}) provide information on the dynamics associated with mid-lying levels of the asymmetric-stretch manifold. Finally, the lowest probe frequencies investigated (1040–958 cm^{-1}) provide a measure of the dynamics of mid and upper vibrational levels along the asymmetric-stretch coordinate. The description of optical-density evolution presented in Figs. 1–3 will be partitioned into three frequency regions consistent with the above discussion. Time constants for the optical-density evolution as a function of probe frequency are summarized for each solvent in Tables I (H_2O), II (D_2O), and III (acetonitrile).

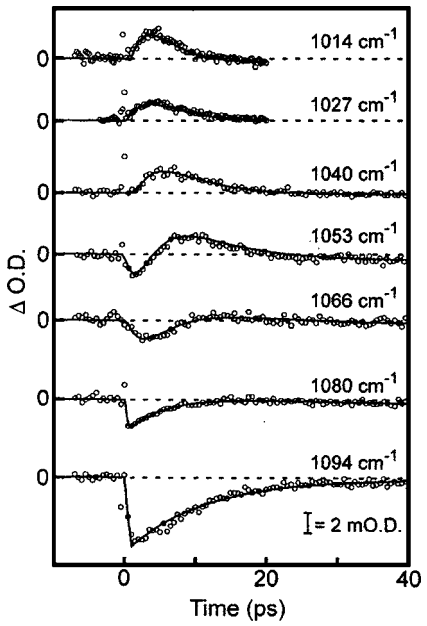

FIG. 1. Evolution in optical density for aqueous OClO following photoexcitation at 401 nm measured at probe frequencies ranging from 1094 to 1014 cm^{-1}. The probe wavelength at which the data were obtained is indicated. The data are presented as the circles, and the solid lines represent the best fit to the data by a sum of exponentials with fit parameters provided in Table I.

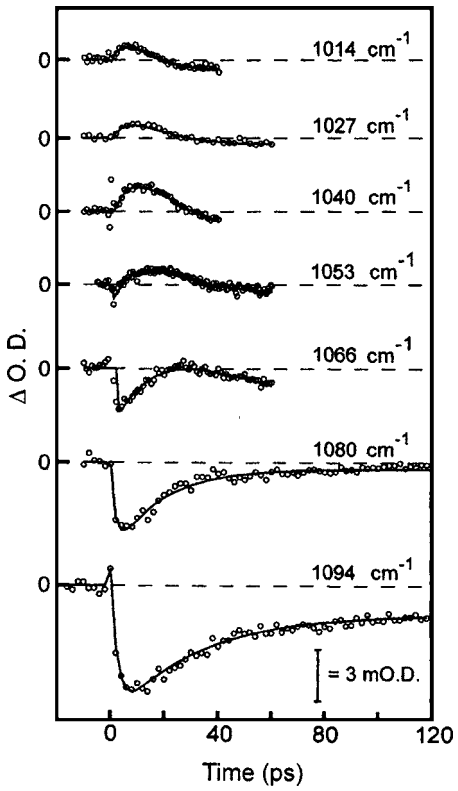

FIG. 2. Evolution in optical density for OClO dissolved in D_2O following photoexcitation at 401 nm measured at probe frequencies ranging from 1094 to 1014 cm^{-1}. The probe wavelength at which the data were obtained is indicated. The data are presented as the circles, and the solid lines represent the best fit to the data by a sum of exponentials with fit parameters provided in Table II.

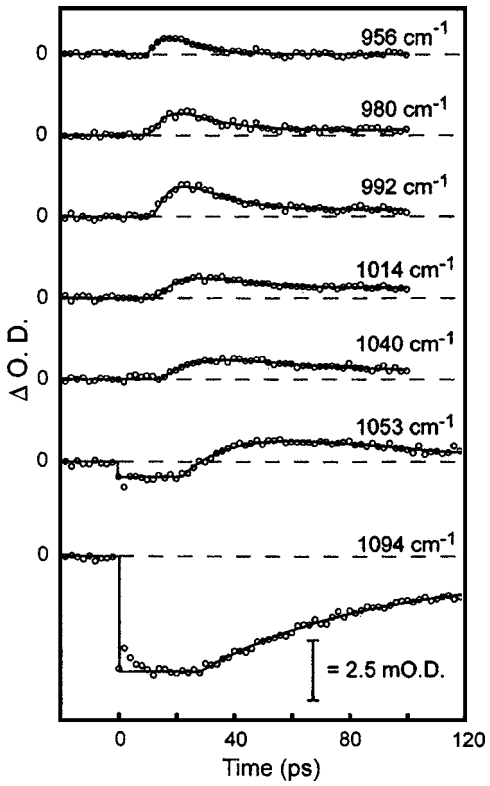

FIG. 3. Evolution in optical density for OClO dissolved in acetnotritile following photoexcitation at 401 nm measured at probe frequencies ranging from 1094 to 952 cm^{-1}. The probe wavelength at which the data were obtained is indicated. The data are presented as the circles, and the solid lines represent the best fit to the data by a sum of exponentials with fit parameters provided in Table III.

1. Probe frequencies of 1094–1080 cm^{-1}

The 1094-cm^{-1} probe is resonant with the $n=0$ to $n=1$ or fundamental transition of the asymmetric stretch; therefore, this frequency provides a measure of depletion and subsequent recovery of ground-state OClO. An initial instrument-response-limited reduction in optical density is observed in all solvents, consistent with the photoinduced depletion of ground-state OClO. In H_2O (Fig. 1), the initial depletion in optical density recovers with a time constant of 9.6±2.0 ps to reveal a small residual depletion of 10±2%, that remains unchanged out to the longest delays investigated (100 ps). This residual depletion provides a measure of photoexcited OClO that results in the formation of OCl and O that escapes the solvent cage, or that results in the production of Cl and O_2. In D_2O (Fig. 2), the pump-induced depletion in optical density recovers with a time constant of 26.3±4.1 ps, roughly three times slower in comparison with H_2O. A persistent depletion in optical density is also observed in D_2O; however, the residual depletion is 23±6% of the initial depletion demonstrating that cage escape and/or atomic chlorine production is enhanced in D_2O relative to H_2O. In acetonitrile (Fig. 3), the pump-induced depletion in optical density is followed by more complex behavior in comparison with H_2O or D_2O. Specifically, the magnitude of the initial depletion remains constant out to 31.7±2.9 ps, then recovers with a time constant of 40±10 ps. The long-time optical-

TABLE I. Kinetic parameters determined from the TRIR study of OClO in H_2O.

$\nu_{pr}(cm^{-1})$[a]	A_1[b]	τ_1 (ps)	A_2	τ_2 (ps)	A_3	τ_3 (ps)[c]
1094	−0.95±0.05	9.6±2.0	···	···	−0.05±0.05	offset
1080	−0.90±0.15	6.9±1.2	···	···	−0.10±0.15	offset
1066	−0.69±0.09	4.5±0.9	0.31±0.09	8.6±2.0	···	···
1053	−0.59±0.08	4.2±1.0	0.41±0.08	7.2±1.2	···	···
1040	−0.51±0.04	3.0±0.9	0.49±0.04	5.1±0.4	···	···
1027	−0.50±0.02	2.7±0.5	0.50±0.02	4.7±1.1	···	···
1014	−0.57±0.16	2.1±0.5	0.43±0.16	4.3±1.2	···	···

[a]Probe frequencies.
[b]Amplitudes are normalized such that $\Sigma_i|A_i|=1$. Errors represent one standard deviation from the mean of all measurements (≥ 4) at a given probe wavelength.
[c]Time constant is set to 10 000 ps to account for residual depletion.

TABLE II. Kinetic parameters determined from the TRIR study of OClO in D_2O.

$\nu_{pr}(cm^{-1})$[a]	A_1[b]	τ_1(ps)	A_2	τ_2(ps)	A_3	τ_3(ps)[c]
1094	−0.90±0.07	26.3±4.1	⋯	⋯	−0.10±0.08	offset
1080	−0.84±0.06	21.7±3.5	⋯	⋯	−0.16±0.06	offset
1066	−0.49±0.01	13.5±1.5	0.46±0.03	18.1±1.1	−0.05±0.03	offset
1053	−0.49±0.01	11.6±2	0.49±0.01	14.5±2	−0.02±0.02	offset
1040	−0.43±0.04	8.5±1.7	0.51±0.02	15.2±3.5	−0.06±0.03	offset
1027	−0.39±0.06	5.9±1.5	0.51±0.02	14.2±3.4	−0.10±0.04	offset
1014	−0.42±0.06	5.8±1.7	0.50±0.01	11.7±3.9	−0.08±0.06	offset

[a]Probe frequencies.
[b]Amplitudes are normalized such that $\Sigma_i|A_i|=1$. Errors represent one standard deviation from the mean of all measurements ($\geqslant 7$) at a given probe wavelength.
[c]Time constant is set to 10 000 ps to account for residual depletion.

density depletion in acetonitrile is 47±16% of the initial depletion, and demonstrates that geminate-recombination efficiency is reduced relative to H_2O and D_2O. Similar behavior was observed in previous UV-visible transient absorption and time-resolved resonance Raman studies.

At 1080 cm^{-1}, both the $n=0$ to $n=1$, and $n=1$ to $n=2$ transitions contribute to the optical-density evolution. In all solvents, an instrument-response-limited reduction in optical density is observed, but the depletion amplitude is reduced relative to that observed at 1094 cm^{-1} consistent with a reduction in the contribution of the fundamental transition to the optical-density evolution as the probe frequency is reduced. The pump-induced depletion of optical density recovers with an enhanced rate relative to 1094 cm^{-1}, consistent with probing higher vibrational states along the asymmetric-stretch manifold. Specifically, in H_2O and D_2O the recovery in optical density occurs with time constants of 6.9±1.2 and 21.7±3.5 ps, respectively. In acetonitrile, the delay in recovery as well as the rate of optical-density depletion recovery is shortened relative 1094 cm^{-1}, with the recovery beginning at 27.7±2.6-ps following photoexcitation, and proceeding with a time constant of 32±8 ps.

2. Probe frequencies of 1066–1053 cm^{-1}

In this frequency region for OClO dissolved in H_2O and D_2O, a small pump-induced reduction in optical density is followed by an increase and subsequent decay in optical density. This evolution in optical density is consistent with the production and subsequent decay of intermediate vibrational levels ($n=2$ to $n=5$) along the asymmetric-stretch coordinate during the vibrational-relaxation process. The evolution in optical density was well fit by a sum of two exponentials corresponding to the initial appearance and subsequent decay of optical density. In H_2O at 1066 cm^{-1}, the optical density appears with a time constant of 4.5±0.9 ps and decays with a time constant of 8.6±2.0 ps. In D_2O at this same frequency, the appearance and decay time constants are 13.5±1.5 and 18.1±1.1 ps, respectively. Similar to the observation at higher probe frequencies, these time constants demonstrate that the vibrational-relaxation rates are two- to threefold reduced in D_2O compared to H_2O. In acetonitrile, the initial pump-induced depletion in optical density persists out to 30.0±1.0 ps followed by an appearance time constant of 25.0±6.0 ps, but no perceptible decay is observed. At 1053 cm^{-1} in H_2O, optical density appears with a time constant of 4.2±1.0 ps and decays with a time constant of 7.2±1.2 ps. The corresponding time constants in D_2O are 11.6±2.0 and 14.5±2.0. Finally, in acetonitrile the initial optical-density depletion persists to 21.8±2.8 ps followed by an appearance of optical density with a time constant of 25.0±6.0 ps and subsequent decay with a time constant of 46±16 ps.

TABLE III. Kinetic parameters determined from the TRIR study of OClO in acetonitrile.

$\nu_{pr}(cm^{-1})$[a]	A_1[b]	τ_1(ps)	A_2	τ_2(ps)	A_3	τ_3(ps)[c]	Dwell
1094	−0.53±0.15	40±10	−0.45±0.15	offset[c]	⋯	⋯	31.7±2.9
1080	−0.80±0.15	32±8	−0.20±0.15	offset	⋯	⋯	27.7±2.6
1066	−0.91±0.09	25±6	0.05±0.11	offset	⋯	⋯	30.0±0.1
1053	0.87±0.09	25±6	0.11±0.12	46±16	⋯	⋯	21.8±2.8
1040	−0.49±0.01	12.8±1	0.46±0.02	23.1±4.5	0.06±0.02	offset	16.3±1.7
1027	−0.48±0.01	8.4±1.1	0.45±0.03	17.1±2.6	0.06±0.04	offset	15.5±1.5
1014	−0.43±0.16	9.3±1.9	0.52±0.18	15.5±2.9	0.05±0.03	offset	15.2±1.8
1000	−0.49±0.1	8.5±1.2	0.47±0.01	13.3±1.4	0.04±0.02	offset	15.4±1.2
992	−0.49±0.01	7.1±0.7	0.47±0.02	14.8±3.1	0.04±0.02	offset	13.3±0.5
980	−0.48±0.01	6.3±1.3	0.47±0.02	12.6±2.3	0.05±0.02	offset	12.8±0.7
969	−0.50±0.02	5.6±1.7	0.49±0.02	10.6±1.7	0.02±0.01	offset	11.2±1.7
958	−0.47±0.05	4.8±1.4	0.52±0.05	9.9±2.9	0.01±0.02	offset	11.9±1.6

[a]Probe frequencies
[b]Amplitudes are normalized such $\Sigma_i|A_1|=1$. Errors represent one standard deviation from the mean of all measurements ($\geqslant 8$) at a given probe wavelength.
[c]Time constant is set to 10 000 ps to account for residual depletion.

3. Probe frequencies ≤1040 cm^{-1}

In this frequency region a pump-induced increase in optical density is observed in all solvents followed by decay. This behavior is consistent with population of higher-energy levels of the asymmetric-stretch vibrational manifold during the geminate-recombination process followed by vibrational relaxation. As the probe frequency is reduced, the time constants associated with the optical-density appearance and decay become smaller, reflecting the increased vibrational-relaxation rates for higher-energy states. In H_2O, the evolution in optical density is well modeled by a sum of two exponentials corresponding to the appearance and decay in optical density, with time constants ranging from 3.0±0.9 and 5.1±0.4 ps, respectively, at 1040 cm^{-1} to 2.1±0.5 and 4.3±1.2 ps, respectively, at 1014 cm^{-1}. In D_2O, the appearance and decay time constants are again increased relative to water, with time constants of 8.5±1.7 and 15.2±3.5 ps, respectively, at 1040 cm^{-1} and 5.8±1.7 and 11.7±3.9 ps, respectively, at 1014 cm^{-1}. In acetonitrile, lower probe frequencies could be employed due to the increased transparency of the solvent relative to H_2O and D_2O. In acetonitrile, a prominent long-time increase in optical density is observed in addition to the optical-density evolution associated with OClO vibrational relaxation. To accurately fit the data, a sum of three exponentials was required with one of the time constants set equal to 10 000 ps to account for the long-time increase in optical density. Consistent with the behavior observed at higher probe frequencies in this solvent, an initial delay before the onset of optical-density evolution is observed. At 1040 cm^{-1}, after a 16.3±1.7-ps delay the optical density increases with a time constant of 12.8±1.0 ps and decays with a 23.1±4.5-ps time constant. At 1014 cm^{-1}, the delay in optical-density evolution is reduced to 15.2±1.8 ps followed by rise and decay times of 9.3±1.9 and 15.5±2.9 ps, respectively. Finally, at 958 cm^{-1}, centered roughly on the $n=12$ to $n=13$ transition, a 11.9±1.6-ps delay in spectrum evolution is followed by optical-density appearance and decay with time constants of 4.8±1.4 and 9.9±2.9 ps, respectively.

B. Modeling of the optical-density evolution

Two models for the vibrational-relaxation dynamics of OClO were employed to analyze the solvent-dependent evolution in optical density described above. The first model employed was used in earlier UV-visible transient absorption studies of OClO dissolved in water and acetonitrile.[10,12] This approach borrows from Landau-Teller theory in which the vibrational-relaxation rate constants are predicted to scale linearly with vibrational level.[35,36] This model assumes that relaxation occurs primarily through collisions with nearby solvent molecules; therefore, we will refer to this model as the "collisional model." The second model investigated also predicts that the vibrational-relaxation rate constants will increase with vibrational level; however, the linear level dependence of the collisional model is augmented by an additional term that describes the frequency dependence of the solvent-solute coupling. We will refer to this model as the "perturbative model." The level dependence of the vibrational-relaxation rate constants for the two models and the comparison of the predicted evolution in optical density derived from these models to experiment are described below.

1. Collisional model

In the collisional model, the level-dependent vibrational-relaxation rate constants are given by[10,12]

$$k_{n\rightarrow n-1} = nk_{1\rightarrow 0}. \tag{1}$$

In the above expression, $k_{n'\rightarrow n-1}$ is the rate constant associated with relaxation between levels n and $n-1$, and $k_{1\rightarrow 0}$ is the relaxation rate constant from level $n=1$ to the $n=0$ ground state. Geminate recombination is assumed to result in initial population of the $n=15$ level along the asymmetric-stretch coordinate. The level populations of the asymmetric-stretch manifold were then calculated using the following master equation:

$$\frac{d\rho_n(t)}{dt} = (n+1)k_{1\rightarrow 0}\rho_{n+1}(t) - nk_{1\rightarrow 0}\rho_n(t). \tag{2}$$

The master equation was solved utilizing Euler's method with a time step of 0.1 ps, and the results of this calculation are the populations of each vibrational level as a function of time. Detailed balance was initially included in this analysis, but it was determined that the reverse process is negligible due to the large energy-level spacings of interest relative to the available thermal energy. The contributions of the individual vibrational-level populations were weighted by the monochromator bandwidth (Gaussian with a 30-cm^{-1} full width at half maximum), and the weighted contributions were summed at a given time delay to produce the predicted evolution in optical density. The predicted evolution was also convolved with the instrument response; however, due to the time scales of interest the effect of convolution was negligible.

2. Perturbative model

Previous MD studies of OClO suggested an alternative description of the vibrational-relaxation dynamics from that of the collisional model.[31–33] In this approach, the linear dependence of the relaxation rate constants on vibrational level is augmented by an additional term corresponding to the frequency dependence of the solute-solvent coupling. In this approach, the level-dependent relaxation rate constants are given by

$$k_{n\rightarrow n-1} = nk_{1\rightarrow 0}\tilde{F}_{q,q'}(\omega)\hbar^{-2}. \tag{3}$$

In this equation, $\tilde{F}_{q,q'}(\omega)$ is the real part of the Fourier transform of the solvent-solute force-force correlation function. In Eq. (3), the linear dependence of the relaxation rate constants on n inherent in the collisional model is retained; however, an additional term is included that takes into account the frequency dependence of the solvent-solute coupling. This additional term has the effect of increasing the rate constants relative to the values predicted by the collisional model. The frequency-dependent coupling was derived using the MD re-

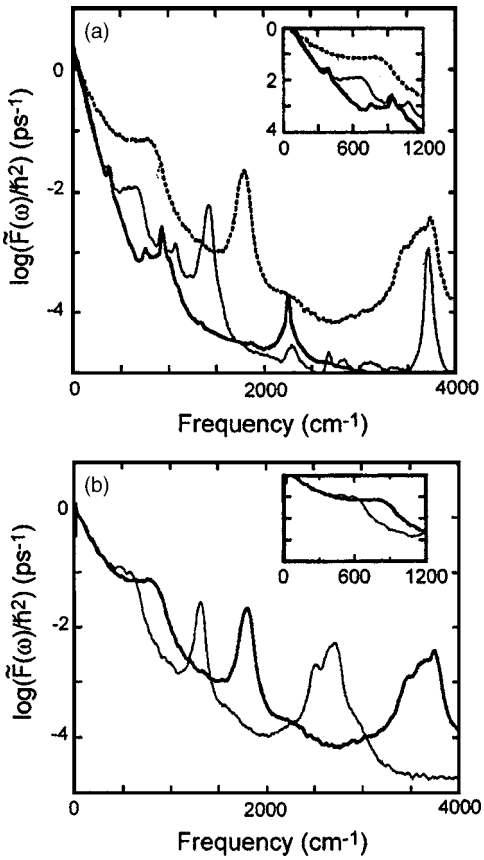

FIG. 4. (A) The variation in the power spectrum of the solvent-solute force-force correlation functions $\tilde{F}(\omega)$ as a function of frequency as reported by Benjamin and co-workers. Spectra are with reference to the asymmetric stretch of OClO in water (dotted line), ethanol (thin line), and acetonitrile (thick line). The figure inset provides an expanded view of the low-frequency region of the power spectrum. (B) The variation in $\tilde{F}(\omega)$ as a function of frequency for H_2O (solid line) and D_2O (dashed line).

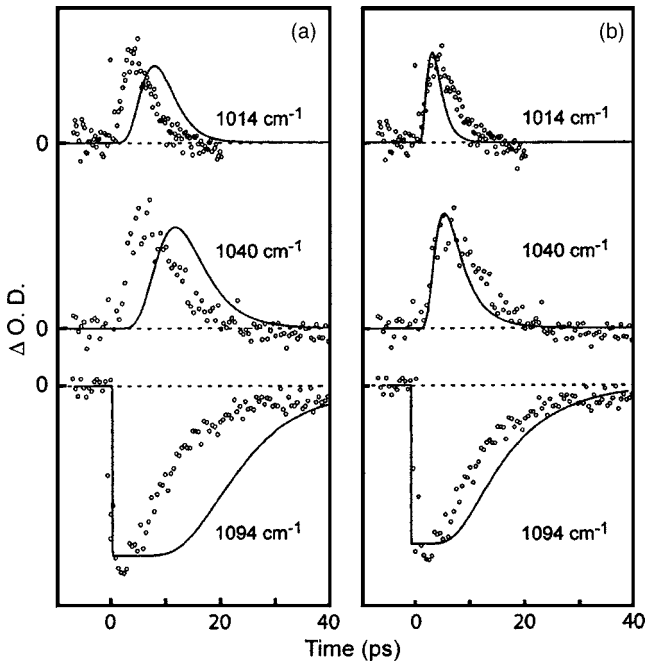

FIG. 5. (A) Comparison of the experimental evolution in optical density of aqueous OClO (circles) to that predicted using the collisional model for vibrational relaxation along the asymmetric-stretch coordinate (solid line). (B) Comparison of the experimental evolution in optical density of aqueous OClO (circles) to that predicted using the perturbation model for describing the vibrational-relaxation dynamics along the asymmetric-stretch coordinate (solid line). Comparisons are presented for probe wavelengths of 1094, 1040, and 1014 cm^{-1} to represent the entire vibrational dynamics across the probed asymmetric-stretch manifold.

sults of Benjamin and co-workers, with their results for the solvents of interest reproduced in Fig. 4.

3. H_2O

Figure 5 presents a comparison between the predicted evolution in optical density derived using the collisional and perturbation models to experiment. Three probe frequencies, 1094, 1040, and 1014 cm^{-1}, were chosen for presentation since they provide a measure of the dynamics that occur in the lower, middle, and upper regions of the asymmetric-stretch vibrational manifold, respectively. In this simulation, $k_{1\rightarrow 0}$ was set equal to 0.105 ps^{-1} consistent with previous work.[10,12,24,25] The collisional model [Fig. 5(A)] demonstrates reasonable agreement with experiment at 1094 cm^{-1}; however, the experimental data do not demonstrate the delay in recovery relative to zero time as predicted by this model. At 1040 and 1014 cm^{-1}, the maximum increase in optical density predicted by the collisional model is delayed relative to experiment. In contrast, the perturbation model [Fig. 5(B)] better reproduces the evolution in optical density. Specifically, the evolution at 1094 cm^{-1} is more accurately reproduced due to the faster relaxation rates for higher vibrational levels predicted by this model. In addition the appearance and decay kinetics of the optical-density evolution at 1040 and 1014 cm^{-1} are reproduced; however, the rate of relaxation at higher levels is slightly overestimated as evidenced by the modest discrepancy between experiment and theory at 1014 cm^{-1}. Although the perturbation model is in qualitative agreement with the measured evolution in optical density, it should be noted that quantitative agreement is not achieved. Specifically, the MD results suggest that $k_{1\rightarrow 0}=0.019$ ps^{-1}, a significant reduction from the value employed here and in previous work.

4. D_2O

Comparison of the vibrational-relaxation dynamics observed in D_2O relative to H_2O provides a good test of the perturbation model since these solvents are structurally similar, the mode frequencies of these solvents are significantly different, and the frequency dependence of the solvent-solute coupling is altered. Reflecting the change in solvent-solute coupling in D_2O relative to H_2O near the frequency of the OClO asymmetric stretch, the MD studies predict that the vibrational-relaxation rate constants should be reduced in D_2O relative to H_2O. Figure 6 presents a comparison of the predicted evolution in optical density derived using the collisional and perturbative models with experiment. The comparisons are performed using a rate constant of $k_{1\rightarrow 0}=0.0385$ ps^{-1} determined using the time constant for optical-density recovery measured at 1094 cm^{-1} (Table II). Similar to the observation in H_2O, the collisional model [Fig. 6(A)] fails to accurately predict the observed evolution in optical density. For example, at 1094 cm^{-1} the collisional model

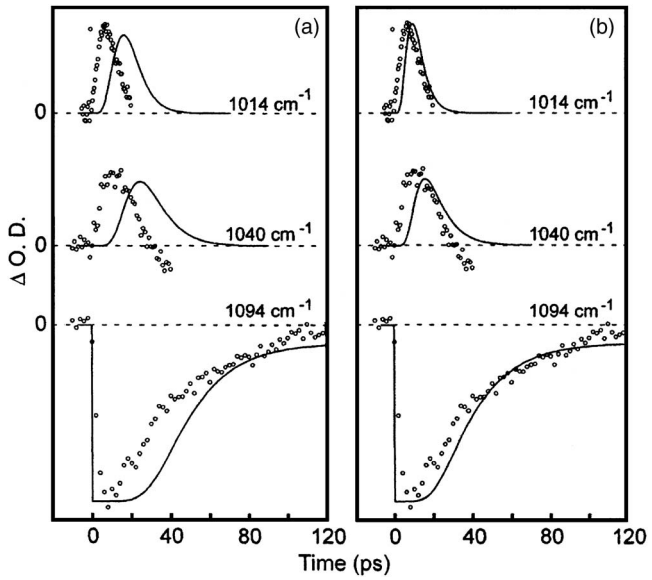

FIG. 6. (A) Comparison of the experimental evolution in optical density of OClO dissolved in D_2O (circles) to that predicted using the collisional model for describing the vibrational-relaxation dynamics along the asymmetric stretch (solid line). (B) Comparison of the experimental evolution in optical density of OClO dissolved in D_2O (circles) to that predicted using the perturbation model for describing the vibrational-relaxation dynamics along the asymmetric stretch (solid line). Comparisons are presented for probe wavelengths of 1094, 1040, and 1014 cm^{-1} to represent the entire vibrational dynamics across the probed asymmetric-stretch manifold.

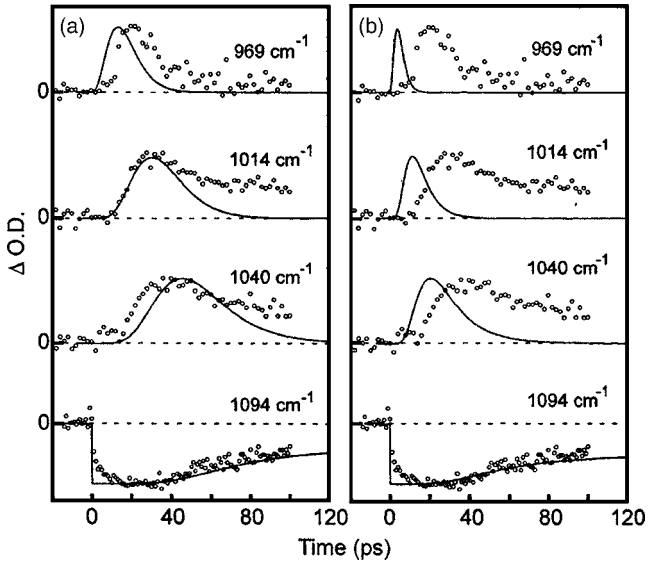

FIG. 7. (A) Comparison of the experimental evolution in optical density of OClO dissolved in acetonitrile (circles) to that predicted using the collisional model for describing the vibrational-relaxation dynamics along the asymmetric stretch (solid line). (B) Comparison of the experimental evolution in optical density of OClO dissolved in acetonitrile (circles) to that predicted using the perturbation model for describing the vibrations-relaxation dynamics along the asymmetric stretch (solid line). Comparisons are presented for probe wavelengths of 1094, 1040, 1014, 992, and 969 cm^{-1} to represent the entire vibrational dynamics across the probed asymmetric-stretch manifold.

predicts a delay in optical-density recovery that is not observed experimentally. Also, the predicted appearance in optical density at 1040 and 1014 cm^{-1} is significantly delayed relative to experiment. These discrepancies indicate that the relaxation rate constants for higher-energy vibrational levels are greater than those predicted by the collisional model. Consistent with this observation, the perturbative model more accurately predicts the experimental optical-density evolution [Fig. 6(B)]. Specifically, at 1094 cm^{-1} a slight delay in optical-density recovery is predicted, but it is not as long as that predicted by the collisional model, and the optical-density recovery is well reproduced. At 1040 and 1014 cm^{-1}, both the location of the maximum increase in optical density and the kinetics associated with the optical-density evolution are well reproduced by the perturbation model.

5. Acetonitrile

Figure 7 presents a comparison of the optical-density evolution predicted using the collisional and perturbative models to experiment. In addition to evolution in optical density observed at 1094, 1040, and 1014 cm^{-1}, a comparison is also presented at 969 cm^{-1} since these data provide a measure of relaxation dynamics for the highest-energy levels of the asymmetric-stretch vibrational manifold. In the modeling, $k_{1\rightarrow 0}$ was set equal to 0.027 ps^{-1}, consistent with previous TRRR and UV-visible transient absorption studies.[12,33] At 1094 cm^{-1}, the collisional model [Fig. 7(A)] reproduces the observed delay in optical-density recovery, but the predicted recovery is slow in comparison with the experiment. At 1040 and 1014 cm^{-1}, the predicted optical-density evolution is in good agreement with experiment, except for the persistent long-time offset in optical density. It will be argued below that this offset arises from vibrational-energy transfer from the asymmetric-stretch coordinate to the methyl rock of acetonitrile. Finally, at 969 cm^{-1} the experimental optical-density evolution occurs on a significantly longer time scale relative to the prediction of the collisional model. In contrast to the case in H_2O and D_2O, the perturbative model does not accurately reproduce the optical-density evolution in acetonitrile [Fig. 7(B)]. At 1094 cm^{-1}, the experimental and predicted evolution in optical density is in good agreement; however, at the 1040, 1014, and 969 cm^{-1} the predicted dynamics occur on a much shorter time scale relative to experiment.

IV. DISCUSSION

The TRIR studies outlined here provide a detailed look into the solvent dependence of the vibrational-energy relaxation dynamics along the asymmetric-stretch coordinate of OClO. The results above demonstrate that following the reformation of ground-state OClO by geminate recombination of the primary O and ClO photofragments, vibrational energy is deposited along the asymmetric-stretch coordinate, and that vibrational energy is lost from this coordinate to the solvent. In H_2O and D_2O, excess vibrational energy appears along the asymmetric-stretch coordinate in ~1-ps following photoexcitation demonstrating that reformation of ground-state OClO occurs on this time scale in these solvents. This is in agreement with the previous transient absorption and TRRR studies which deduced that ground-state reformation occurs on the subpicosecond time scale.[10,12,24,25]

Comparison of the vibrational-relaxation dynamics observed in H_2O and D_2O provides a good test of the theoretical models of OClO vibrational relaxation given the limited structural differences between these solvents yet substantial differences in frequency associated with solvent degrees of freedom. The success of the perturbative model in reproducing the experimental optical-density evolution in H_2O and D_2O demonstrates that frequency dependence of the solvent-solute coupling is an important factor in defining the vibrational-relaxation rates of OClO in aqueous solution. The MD studies predict that the vibrational-relaxation rate in D_2O is reduced relative to H_2O by a factor-of 1.3 due to modification of the solvent-solute force-force correlation function in the frequency region of the asymmetric-stretch fundamental transistion.[33] Consistent with this expectation, an approximately threefold reduction in rate in D_2O relative to H_2O is observed. Although qualitative agreement with theory is observed, quantitative agreement is obtained only if the relaxation rates in both solvents are increased by approximately fivefold relative to the theoretical values. This discrepancy suggests that the intermolecular potentials used in the MD simulations for OClO in aqueous solution underestimate the magnitude of the OClO-solvent coupling. This discrepancy was observed in earlier MD studies in which quantitative reproduction of the vibrational-relaxation kinetics was achieved by increasing the charges on the Cl and O atoms to values that were substantially larger than those supported by the dipole moment of OClO. The increase in charge has the effect of enhancing the magnitude of the electrostatic coupling between solvent and OClO thereby increasing the relaxation rate.[33]

A second difference in the photochemical reaction dynamics observed in H_2O and D_2O is the reduction in the geminate-recombination quantum yield in D_2O. Previous studies of geminate recombination for other solutes dissolved in H_2O and D_2O have not observed a difference in the recombination quantum yield. For example, visible pump probe studies of O_3^- found no variation in the geminate-recombination yield and dynamics between H_2O and D_2O.[37] One explanation for the reduction in the geminate-recombination quantum yield in D_2O is that the reduced vibrational-relaxation rate in this solvent provides for a corresponding increase in the rate of dissociation. Benjamin and co-workers have suggested that if the dissociation occurs over an energy barrier along the optically prepared $^2A_2$ surface, then excess vibrational energy should promote dissociation.[32] Similar reasoning can be applied to dissociation on the ground $^2B_1$ surface. Specifically, if initially formed ground-state OClO is capable of proceeding along the reaction coordinate towards dissociation to form ClO and O, then excess vibrational energy could promote dissociation. In summary, the reduction of the geminate-recombination quantum yield in D_2O relative to H_2O may simply reflect the variation in the vibrational-relaxation rate between these solvents.

In comparison with H_2O and D_2O, the geminate-recombination and vibrational-relaxation dynamics of OClO in acetonitrile are significantly more complicated. Most notably, there is a substantial delay between photoexcitation and the appearance of excess vibrational energy along the asymmetric-stretch coordinate. Even when probe frequencies resonant with the highest-energy levels along the asymmetric-stretch coordinate are employed, the appearance of vibrational energy is delayed 10-ps relative to photoexcitation. This observation stands in contrast to H_2O and D_2O where at the lowest probe frequencies employed ($1014\ cm^{-1}$) that provide a measure of the population dynamics for intermediate vibrational-energy levels, optical-density increases consistent with vibrational-energy deposition are observed in $\sim$1-ps following photoexcitation. This observation suggests that there is a delay in population of the ground state in acetonitrile relative to H_2O and D_2O. At this juncture, it is useful to revisit the proposed sequence of events that occur following OClO photoexcitation. Photoexcitation results in population of the $^2A_2$ state which undergoes internal conversion to the $^2A_1$ excited state, and this state undergoes subsequent internal conversion to the lower-energy $^2B_2$ excited state. Therefore, the delay in the appearance of vibrational energy along the asymmetric-stretch coordinate in acetonitrile could reflect a reduced rate of internal conversion to the ground state from the $^2B_2$ state. Another possibility is that upon reformation of ground-state OClO by geminate recombination, vibrational energy is initially deposited into a local mode of OClO, presumably a mode of substantial Cl–O stretch chararcter, and that the $\sim$10-ps appearance time for energy along the asymmetric-stretch coordinate reflects intramolecular-vibrational reorganization. This would imply that energy localization only occurs at the very top of the asymmetric-stretch manifold, an idea that is consistent with mode-bifurcation theory.[38,39] However, the observation that vibrational levels up to $n=12$ are populated in acetonitrile demonstrates that only a modest amount of energy ($\sim 3000\ cm^{-1}$) can be lost from the local mode to the solvent in the first 10-ps following geminate recombination.

A second unique aspect of the relaxation dynamics observed in acetonitrile is the inability of the perturbative model to adequately reproduce the level dependence of the vibrational-relaxation rate constants. Given the success of this model in describing the relaxation dynamics in H_2O and D_2O, this result is quite surprising. One reason for this discrepancy may be the substantial delay in internal conversion to the ground state. To explore this possibility, the perturbative model was modified to include a 10-ps delay before population of the $n=15$ state. Even with this delay, the vibrational-relaxation rate constants predicted by the perturbation model were incapable of reproducing the observed evolution in optical density in acetonitrile. Therefore, the values of $\tilde{F}_{q,q'}(\omega)$ [Eq. (3)] were determined by fitting the experimental evolution, and comparison of the experimental and predicted evolution in optical density obtained from this procedure is shown in Fig. 8. Figure 9 presents a comparison of the fit values for $\tilde{F}_{q,q'}(\omega)$ to those obtained from MD. This comparison demonstrates that for higher-energy vibrational level ($n>9$), the MD results overestimate the relaxation rates while the relaxation rates for mid- and lower-energy levels ($n=2$ through $n=7$) are underestimated. Interestingly, the frequency range over which the MD values for $\tilde{F}_{q,q'}(\omega)$

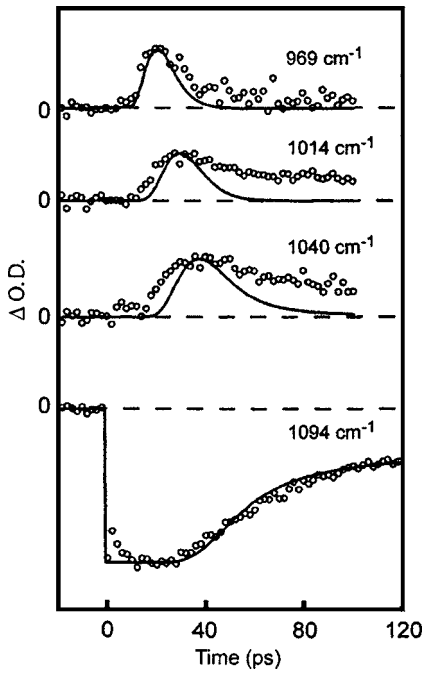

FIG. 8. Comparison of the experimental evolution in optical density of OClO dissolved in acetonitrile (circles) to that determined by fitting the rate constants for the vibrational relaxation dynamics along the asymmetric stretch (solid line). Comparisons are presented for probe wavelengths of 1094, 1040, 1014, and 969 cm^{-1}.

are less than those determined by fitting correspond to the frequency region where the acetonitrile methyl rock is localized. This observation suggests that the MD simulations may underestimate the coupling between the asymmetric stretch of OClO and this solvent mode. This observation suggests that quantum-mechanical effects not included in the classical MD treatment are important in describing the relaxation dynamics of OClO in acetonitrile.

One final aspect of the optical-density evolution in acetonitrile is the long-time offset in optical density observed for the probe frequencies between 1040 and 1014 cm^{-1}. We attribute this offset to the transfer of vibrational energy from

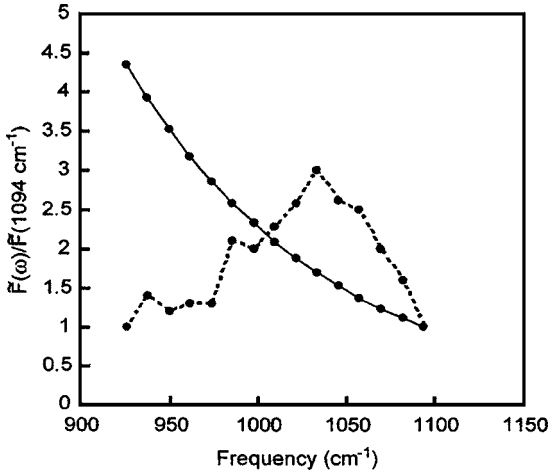

FIG. 9. Comparison of the values for $\tilde{F}_{q,q'}(\omega)$. The solid line represents the values obtained from the MD study while the dashed line represents the values obtained from the manual adjustment of vibrational relaxation rates to obtain the best fit. The values are shown relative to $\tilde{F}_{q,q'}(1094\ cm^{-1})$.

the asymmetric-stretch coordinate of OClO to the methyl rock of acetonitrile. The fundamental transition of methyl rock has a significant IR absorption cross section, and time-resolved Raman studies have placed the vibrational lifetime of the $n=1$ state of the methyl rock at >100 ps.[40] Both the significant absorption of the methyl rock fundamental transition as well as the literature of the $n=1$ state are consistent with assignment of the long-time optical density increase to the methyl rock.

V. CONCLUSIONS

We have performed a series of TRIR absorption studies of OClO dissolved in H_2O, D_2O, and acetonitrile. Following photoexcitation, the evolution in optical density was monitored at frequencies ranging from 1094 to 956 cm^{-1} to investigate the solvent dependence of geminate-recombination and vibrational-relaxation dynamics involving the asymmetric-stretch coordinate. In both H_2O and D_2O, population of mid-lying energy levels ($n=8$) along the asymmetric-stretch coordinate in ~1-ps following photoexcitation demonstrating that geminate recombination occurs on this time scale in aqueous solution. The level-dependent vibrational-relaxation rate constants were approximately threefold reduced in D_2O relative to H_2O in qualitative agreement with the predictions of MD. In both H_2O and D_2O, the vibrational-relaxation kinetics was well modeled by considering the solvent-solute force-force correlation function derived from MD. The geminate-recombination quantum yield is reduced in D_2O relative to H_2O, potentially reflecting the slower vibrational relaxation dynamics in D_2O leading to an increased rate of dissociation. In acetonitrile, the appearance of ground-state population along the asymmetric-stretch coordinate is delayed by ~10-ps relative to photoexcitation. This delay was assigned to a longer lived excited state of OClO in acetonitrile relative to H_2O and D_2O. In contrast to H_2O and D_2O, the vibrational-relaxation rate constants predicted by MD did not reproduce the experimental evolution in optical density. Modification of the frequency-dependent solvent-solute coupling predicted by MD was required to reproduce the vibrational-relaxation dynamics. This modification suggests that quantum-mechanical effects not included in MD are important in describing the relaxation dynamics of OClO in acetonitrile.

ACKNOWLEDGMENTS

The National Science Foundation is acknowledged for their support of this work (CHE-0350191). Acknowledgment is also made to the donors of the Petroleum Research Fund, administered by the American Chemical Society. One of the authors (I.C.B.) gratefully acknowledges support from the Rabinovich Fund administered by the Department of Chemistry at the University of Washington.

[1] S. C. Hayes, C. C. Cooksey, P. M. Wallace, and P. J. Reid, J. Phys. Chem. **105**, 9819 (2001).
[2] F. S. Rowland, Annu. Rev. Phys. Chem. **42**, 731 (1991).
[3] V. Vaida and J. D. Simon, Science **268**, 1443 (1995).
[4] E. C. Richard and V. Vaida, J. Chem. Phys. **94**, 163 (1991).
[5] H. F. Davis and Y. T. Lee, J. Chem. Phys. **105**, 8142 (1996).

[6] E. Bishenden and D. J. Donaldson, J. Chem. Phys. **101**, 9565 (1994).
[7] V. Vaida, G. J. Frost, L. A. Brown, R. Naaman, and Y. Hurwitz, Ber. Bunsenges. Phys. Chem. **99**, 371 (1995).
[8] W. G. Lawrence, K. C. Clemitshaw, and V. A. Apkarian, J. Geophys. Res. **95**, 18591 (1990).
[9] C. L. Thomsen, M. P. Philpott, S. C. Hayes, and P. J. Reid, J. Chem. Phys. **112**, 505 (2000).
[10] J. A. Poulsen, C. L. Thomsen, S. R. Keiding, and J. Thogersen, J. Chem. Phys. **108**, 8461 (1998).
[11] J. Thogersen, C. L. Thomsen, J. A. Poulsen, and S. R. Keiding, J. Phys. Chem. A **102**, 4186 (1998).
[12] M. J. Philpott, S. C. Hayes, and P. J. Reid, Chem. Phys. **236**, 207 (1998).
[13] Y. J. Chang and J. D. Simon, J. Phys. Chem. **100**, 6406 (1996).
[14] R. C. Dunn, B. N. Flanders, and J. D. Simon, J. Phys. Chem. **99**, 7360 (1995).
[15] C. J. Pursell, J. Conyers, and C. Denison, J. Phys. Chem. **100**, 15450 (1996).
[16] C. J. Pursell, J. Conyers, P. Alapat, and R. Parveen, J. Phys. Chem. **99**, 10433 (1995).
[17] H. S. P. Mueller and H. Willner, J. Phys. Chem. **97**, 10589 (1993).
[18] A. Arkell and I. Schwager, J. Am. Chem. Soc. **89**, 5999 (1967).
[19] C.-P. Liu, L.-H. Lai, Y.-Y. Lee, S.-C. Hung, and Y.-P. Lee, J. Chem. Phys. **109**, 978 (1998).
[20] C.-P. Liu, L.-H. Lai, Y.-Y. Lee, S.-C. Hung, and Y.-P. Lee, J. Chem. Phys. **109**, 978 (1998).
[21] J. Thogersen, P. U. Jepsen, C. L. Thomsen, J. A. Poulsen, J. R. Byberg, and S. R. Keiding, J. Phys. Chem. A **101**, 3317 (1997).
[22] M. J. Philpott, S. Charalambous, and P. J. Reid, Chem. Phys. Lett. **281**, 1 (1997).
[23] H. Fidder, F. Tschirschwitz, O. Duhr, and E. T. J. Nibbering, J. Chem. Phys. **114**, 6781 (2001).
[24] C. C. Cooksey and P. J. Reid, Photochem. Photobiol. **80**, 386 (2004).
[25] S. C. Hayes, M. J. Philpott, and P. J. Reid, J. Phys. Chem. A **103**, 5534 (1999).
[26] S. Gnanakaran and R. M. Hochstrasser, J. Chem. Phys. **105**, 3486 (1996).
[27] R. Rey and J. T. Hynes, J. Chem. Phys. **108**, 142 (1998).
[28] P. Hamm, M. Lim, and R. M. Hochstrasser, J. Chem. Phys. **107**, 10523 (1997).
[29] D. A. V. Kliner, J. C. Alfano, and P. F. Barbara, J. Chem. Phys. **98**, 5375 (1993).
[30] M. Lim, S. Gnanakaran, and R. M. Hochstrasser, J. Chem. Phys. **106**, 3485 (1997).
[31] J. Poulsen, T. M. Nymand, and S. R. Keiding, Chem. Phys. Lett. **343**, 581 (2001).
[32] I. Chorny, J. Vieceli, and I. Benjamin, J. Chem. Phys. **116**, 8930 (2002).
[33] I. Chorny, J. Vieceli, and I. Benjamin, J. Chem. Phys. **116**, 8904 (2002).
[34] J. C. Bolinger, S. C. Hayes, T. J. Bixby, and P. J. Reid, J. Chem. Phys. **100**, 4795 (2004).
[35] L. Landau and E. Teller, Phys. Z. Sowjetunion **10**, 34 (1936).
[36] D. J. Nesbitt and J. T. Hynes, J. Chem. Phys. **77**, 2130 (1982).
[37] P. K. Walhout, C. Silva, and P. F. Barbara, J. Phys. Chem. **100**, 5188 (1996).
[38] Z. Lu and M. E. Kellman, J. Chem. Phys. **107**, 1 (1997).
[39] G. M. Schmid, S. L. Coy, R. W. Field, and R. J. Silbey, J. Chem. Phys. **101**, 2869 (1994).
[40] J. C. Deak, L. K. Iwaki, and D. D. Dlott, J. Phys. Chem. A **102**, 8193 (1998).